Hybrid Backstepping Predictive Direct Power Control of Grid Connected 3-Phase 3-Level PVG-UPQC Based on Optimised SVM Technique for Power Quality Improvement

Mazouz Lakhdar[a,*], Dahdouh Adel[b], Brahim ElkhalilYoucefa[c]

[a,b,c]Applied Automation and Industrial Diagnostics Laboratory, Djelfa University,17000 Djelfa, Algeria

l.mazouz@univ-djelfa.dz, Adel.dahdouh@univ-djelfa.dz, khalilyoucefa@gmail.com

***Abstract*—The following paper describes a hybridback stepping-based predictive direct power control strategy for a solar generator and a unified power quality conditioner (UPQC) (GPV). The PVG-UPQC is used for improving power quality and integrating renewable energy at the same time. Harmonics brought on by nonlinear loads in both current and voltage is reduced and in the same time it is used for compensating reactive power. The solar generator's dc bus joins series and shunt active power filters to create the PVG-UPQC. The shunt filter decreases harmonic current while acting as a source of current. By acting as a voltage source, the series filter adjusts for voltage harmonics and changes like voltage sag/swell.A hybrid control approach based on back stepping-PDPC coupled with a SVM controller is developed in order to develop the performance of PVG-UPQC.The DC capacitor voltage balancing is based on an energy-minimization strategy. The objectives include eliminating voltage and current harmonics while keeping acceptable dynamic response, as well as delivering compensation signals more quickly and accurately under a range of load circumstances. Simulation results from Matlab/Simulink for a nonlinear load are used to verify the proposed control strategy efficiency. These results demonstrate the superiority and potency of the BC-PDPC regulator when compared to those obtained with a linear PI controller. Index Terms—Power quality, PV generator, UPQC, Backsteppingcontroller, space vector modulation (SVM).**

NOMENCLATURE

Abbreviation

PDPC	Predictive Direct Power Control
BC	Backstepping Controller
PVG	PhotoVoltaic Generator
THD	Total Harmonic Distortion

I. INTRODUCTION

Power quality has declined due to harmonic production as a result of the increased use of power electronic devices in recent years [1].The vocabulary and standards for power quality have been fully defined inIEC-555 and IEEE-519. The previous standards require that the permitted overall harmonic distortion is around 5% [2]. By using passive filters, the abovementioned problems can be somewhat resolved [3-6]. The load current and voltage waveforms' random oscillations would not be eliminated by this kind of filter, though. Instead, compensating devices such hybrid filters, parallel active filters, series active filters, and static variable compensators (SVC, PAF, SAF) are advised to guarantee the quality of power [7]. However, they can only solve one or two power quality concerns, which frequently limit their capacities. Recent works has shown that unified power quality conditioners, which have both series and shunt active filters, can simultaneously address most power quality problems [8].

The UPQC can keep voltage sags and swells out of the system while maintaining a constant load end-voltage [9]. Furthermore, the UPQC can efficiently provide the load's reactive power necessities and contain generated load harmonic currents, avoiding them from returning to the efficacy and interrupting customers' voltage and current [10].

A variety of UPQC control procedures have been given in the literature review. A practical energy storage system based on UPQC is shown in [11] to control the oscillations of power under unbalanced voltage circumstances at the same time . In actuality, the results reported in this research do not clearly demonstrate the voltage's THD. The controller utilized in the article [12] is a conventional PI regulator, in which a three-phase solar PV and battery energy storage system integrated UPQC, the results shown are insufficient, and the length of the simulation cannot demonstrate the flexibility of the controller.

The DC bus voltage as well as the active and reactive power variations have shown the inadequacy of the suggested control proposed in [13] in which authors in this paper present an inductive hybrid UPQC for Power quality management. A system for improving power quality in solar power systems that are connected to the grid utilizing UPQC has been documented in [14]. Other than the high value of the THD, which reached 4.66%, the system does not demonstrate the controller's abilities under nonlinear changes.

With the aim of filtering active and reactive powers within nonlinear load changes and improving power quality and fluctuations of current and voltage harmonics variations like voltage sag/swell compensations, a novel control procedure based on a BPDPC-SVM technique for the PVG-UPQC is presented in this paper to address the shortcomings of the aforementioned literature papers. Additionally, using various simulation results for a nonlinear load, a proposed work in

which conventional PI control is used to make comparative study in order to verify the suggested controller's strength and effectiveness. The suggested regulation system, which ensures an excellent level of power quality on the grid based on the Introduced BPDPC-SVM regulator, has been successfully shown along with the obtained decreased THD for current and voltage harmonic compensations as well as less fluctuations on the DC link.

The remainder of the paper is divided into: part II details the configuration of various sections of the PVG-UPQC, part III provides results and also their interpretations, and part IV reflects the conclusion of the current study.

II. CONFIGURATION OF CONTROL

The fundamental functioning of the recommended control strategy for the PVG-UPQC connected to a nonlinear load is shown in Figure 1. The switch control signals are generated via a three-level space vector modulator. The voltage references for the SVM are provided by the feedback linearization controllers. The harmonic references are established using the instantaneous PQ theory for currents and PQ-PLL for voltages [17–19]. Compensation objectives can be obtained consist of reactive power compensation, current and voltage harmonics reduction, and DC bus management for the duration of the exchange of bidirectional active power between two active filters, power grid and the PV generator.

2.1 GPV-UPQC Mathematical Model

A differential equation that is formulated in α-β stationary frame describes the dynamic model of the PVG-UPQC. Equations (1) and (3) present this model.

$$\frac{di_{fp\alpha}}{dt} = -\frac{R_{fp}}{L_{fp}} i_{fp\alpha} - \frac{v_{s\alpha}}{L_{fp}} + \frac{v_{fp\alpha}}{L_{fp}}$$
$$\frac{di_{fp\beta}}{dt} = -\frac{R_{fp}}{L_{fp}} i_{fp\beta} - \frac{v_{s\beta}}{L_{fp}} + \frac{v_{fp\beta}}{L_{fp}} \quad (1)$$

The parallel filter's output powers are provided as follows:

$$\begin{bmatrix} P_{fp} \\ Q_{fp} \end{bmatrix} = \begin{bmatrix} v_{fp\alpha} & v_{fp\beta} \\ v_{fp\beta} & -v_{fp\alpha} \end{bmatrix} \begin{bmatrix} i_{fp\alpha} \\ i_{fp\beta} \end{bmatrix} \quad (2)$$

The derivative of powers is calculated using (1) and (2) and The Lie derivative technique as follows:

$$\frac{dP_{fp}}{dt} = \frac{1}{L_{fp}} \left(-R_{fp} P_{fp} + V_{fp\alpha} \right)$$
$$\frac{dQ_{fp}}{dt} = \frac{1}{L_{fp}} \left(-R_{fp} Q_{fp} + V_{fp\beta} \right) \quad (3)$$

in which :

$$V_{fp\alpha} = v_{s\alpha} v_{fp\alpha} + v_{s\beta} v_{fp\beta} - \left(v_{s\alpha}^2 + v_{s\beta}^2 \right)$$
$$V_{fp\beta} = -v_{s\beta} v_{fp\alpha} + v_{s\alpha} v_{fp\beta} \quad (4)$$

It may also be expressed in writing form (5).

$$\dot{x}_p = f_p(x_p) + g_p(x_p) u_p \quad (5)$$

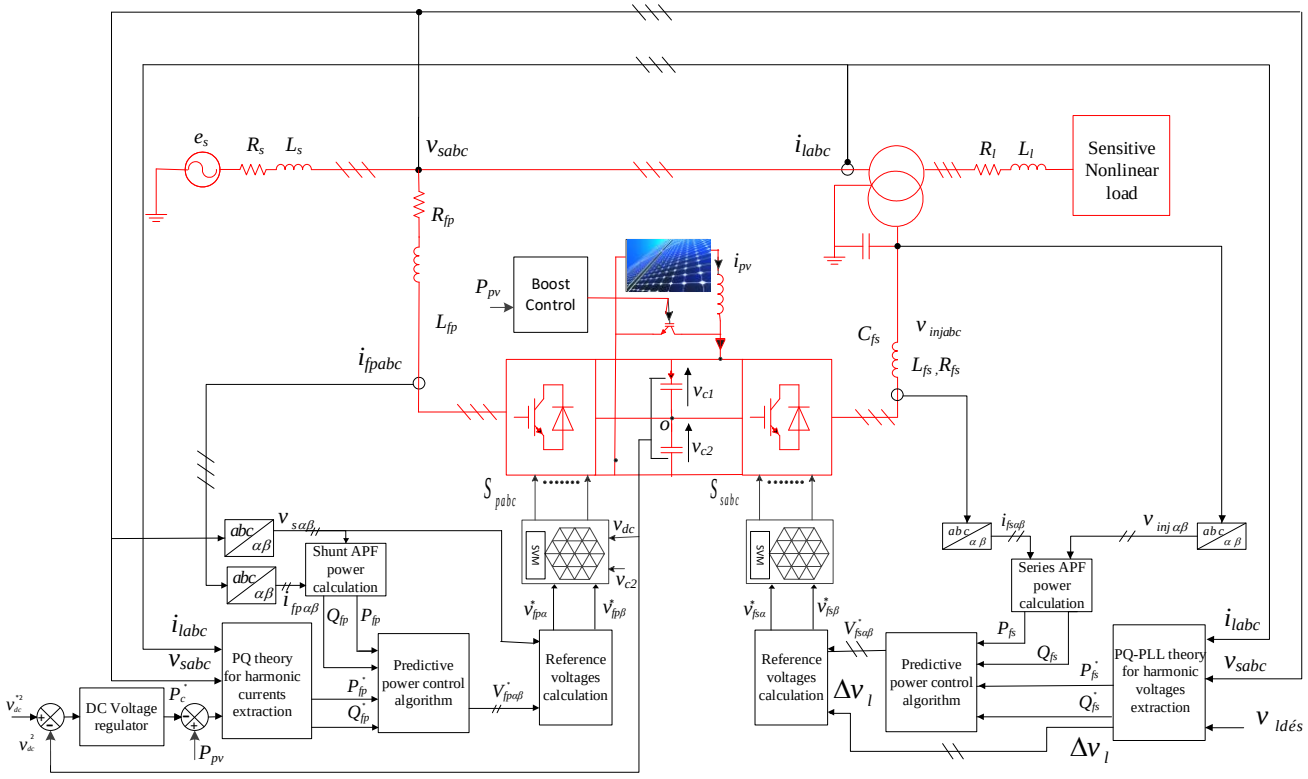

Fig. 1. Back stepping- PDPC control scheme of the PVG-UPQC.

where:

$$f_p(x_p)=\begin{bmatrix}-\frac{R_{fp}}{L_{fp}}x_{p1}\\ -\frac{R_{fp}}{L_{fp}}x_{p2}\end{bmatrix}, g_p(x_p)=\begin{bmatrix}\frac{1}{L_{fp}} & 0\\ 0 & \frac{1}{L_{fp}}\end{bmatrix}, x_p=\begin{bmatrix}P_{fp}\\ Q_{fp}\end{bmatrix}, u_p=\begin{bmatrix}V_{fp\alpha}\\ V_{fp\beta}\end{bmatrix}$$

$$y_p=\begin{bmatrix}y_{p1}\\ y_{p2}\end{bmatrix}=\begin{bmatrix}h_{p1}\\ h_{p2}\end{bmatrix}$$

The shunt filter's voltages, active power, and reactive power are designated as $V_{fp\alpha\beta}$, $P_{fp}$and Q_{fp}, respectively.

the DC-Bus is expressed as:

$$\frac{dv_{dc}^{2}}{dt}=\frac{2P_c}{C_{dc}} \tag{6}$$

Additionally, it may be stated as (7).

$$\dot{x}_{dc}=f_{dc}(x_{dc})+g_{dc}(x_{dc})u_{dc} \tag{7}$$

Where: $f_{dc}(x_{dc})=0$, $g_{dc}(x_{dc})=\frac{2}{C_{dc}}$ and $u_{dc}(x_{dc})=P_c$

The model of a serial filter is:

$$\begin{aligned}\frac{di_{fs\alpha}}{dt}&=-\frac{R_{fs}}{L_{fs}}i_{fs\alpha}-\frac{v_{inj\alpha}}{L_{fs}}+\frac{v_{fs\alpha}}{L_{fs}}\\ \frac{di_{fs\beta}}{dt}&=-\frac{R_{fp}}{L_{fs}}i_{fs\beta}-\frac{v_{inj\beta}}{L_{fs}}+\frac{v_{fs\beta}}{L_{fs}}\end{aligned} \tag{8}$$

The derivative of powers is presented as follows like the preceding system:

$$\begin{aligned}\frac{dP_{fs}}{dt}&=\frac{1}{L_{fs}}\left(-R_{fs}P_{fs}+V_{fs\alpha}\right)\\ \frac{dQ_{fs}}{dt}&=\frac{1}{L_{fs}}\left(-R_{fs}Q_{fs}+V_{fs\beta}\right)\end{aligned} \tag{9}$$

Where

$$\begin{aligned}V_{fs\alpha}&=v_{inj\alpha}v_{fs\alpha}+v_{inj\beta}v_{fs\beta}-\left(v_{inj\alpha}^2+v_{inj\beta}^2\right)\\ V_{fs\beta}&=-v_{inj\beta}v_{fs\alpha}+v_{inj\alpha}v_{fs\beta}\end{aligned} \tag{10}$$

The series filter model is:

$$\dot{x}_s=f_s(x_s)+g_s(x_s)u_s \tag{11}$$

Where:

$$f_s(x_s)=\begin{bmatrix}\frac{1}{C_{fs}}x_{s1}\\ \frac{1}{C_{fs}}x_{s2}\end{bmatrix}, g_s(x_s)=\begin{bmatrix}\frac{1}{L_{fs}} & 0\\ 0 & \frac{1}{L_{fs}}\end{bmatrix}, x_s=\begin{bmatrix}P_{fs}\\ Q_{fs}\end{bmatrix}, u_s=\begin{bmatrix}V_{fs\alpha}\\ V_{fs\beta}\end{bmatrix}$$

$$y_s=\begin{bmatrix}y_{s1}\\ y_{s2}\end{bmatrix}=\begin{bmatrix}h_{s1}\\ h_{s2}\end{bmatrix}$$

The series filter's voltages, active power, and reactive power are designated as$V_{fs\alpha\beta}$, P_{fs} *and* Q_{fs}

As shown in Figure 2, the solar generator's (PVG) output is coupled to a boost converter.

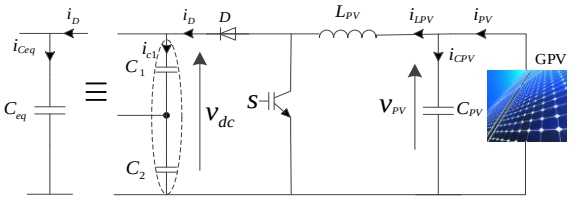

Fig. 2. PV Generator boost converter.

The dynamic equations below represent the state space model for this converter:

$$\begin{aligned}\frac{dv_{pv}}{dt}&=\frac{1}{C_{pv}}i_{pv}-\frac{1}{C_{pv}}i_{Lpv}\\ \frac{di_{Lpv}}{dt}&=\frac{1}{L_{pv}}v_{pv}-\frac{1}{L_{pv}}v_{dc}\end{aligned} \tag{12}$$

The boost's average model changes to the following model when D is specified as duty cycle:

$$\begin{aligned}\frac{di_{Lpv}}{dt}&=\frac{1}{L_{pv}}v_{pv}-\frac{1}{L_{pv}}(1-D)v_{dc}\\ \frac{dv_{pv}}{dt}&=\frac{1}{C_{pv}}i_{pv}-\frac{1}{C_{pv}}i_{Lpv}\end{aligned} \tag{13}$$

The following form can be used to express the equations:

$$\dot{x}_b=f_b(x_b)+g_b(x_b)u_b \tag{14}$$

In which:

$$f_b(x_b)=\begin{bmatrix}\frac{1}{L_{pv}}v_{pv}\\ \frac{1}{C_{pv}}i_{pv}\end{bmatrix}, g_b(x_b)=\begin{bmatrix}-\frac{1}{L_{fp}} & 0\\ 0 & -\frac{1}{C_{pv}}\end{bmatrix}, x_b=\begin{bmatrix}i_{Lpv}\\ v_{pv}\end{bmatrix}, u_b=\begin{bmatrix}v_{dc}\\ i_{Lpv}\end{bmatrix}$$

$$y_b=\begin{bmatrix}y_{b1}\\ y_{b2}\end{bmatrix}=\begin{bmatrix}h_{b1}\\ h_{b2}\end{bmatrix}$$

2.2 Detection method for MPPT

In solar PV systems, the PV panel voltage at a particular level despite maximizing power [5] is increased and also regulated by using the DC-DC boost converter in which it is controlled by an MPPT controller.

The P&O detection technique is used in this work due to its ease of use and affordable implementation[7]. Fig. 6 shows the P&O detection algorithm's flowchart.

For objective to evaluate the power of output before and after the disturbance, The PV generator's operating point can be changed using the Perturb & Observe method by increasing or decreasing the boost converter's duty cycle. When the power increases, the algorithm disturbs the structure in the similar direction; otherwise, it perturbs the structure in the opposite way. Four potential choices are offered during the MPPT's tracking, as seen in Fig. 3.

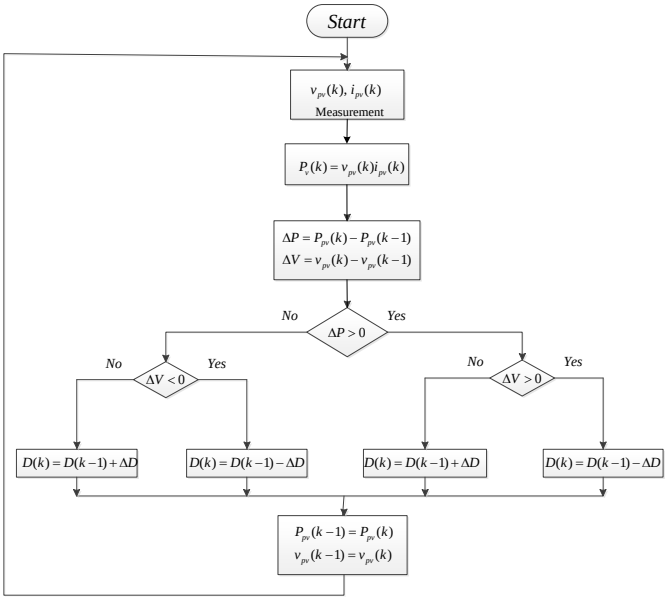

Fig. 3. P&O detection algorithm

2.3 Extraction of Harmonic

Performance of the active filter is significantly impacted by the identification technique utilized to eliminate harmonics from disturbed waveforms [10], [19]. The methods used to extract harmonics are explained in the following sections.

A. Extraction of harmonic currents using PQ hypothesis

This study employs the instantaneous power hypothesis technique as shown in Fig. 4.

The instantaneous powers of the load are calculated as follows:

$$\begin{bmatrix} P_l \\ Q_l \end{bmatrix} = \begin{bmatrix} v_{s\alpha} & v_{s\beta} \\ v_{s\beta} & -v_{s\alpha} \end{bmatrix} \begin{bmatrix} i_{l\alpha} \\ i_{l\beta} \end{bmatrix} \tag{15}$$

The following is a possible way to express the powers:

$$\begin{cases} P_l = \bar{P}_l + \tilde{P}_l \\ Q_l = \bar{Q}_l + \tilde{Q}_l \end{cases} \tag{16}$$

The total reactive power along ($\bar{Q}_l$ and $\tilde{Q}_l$ components) with the oscillatory component of active power ($\tilde{P}_l$) are chosen as compensatory power references for reducing harmonics and compensating for reactive power.

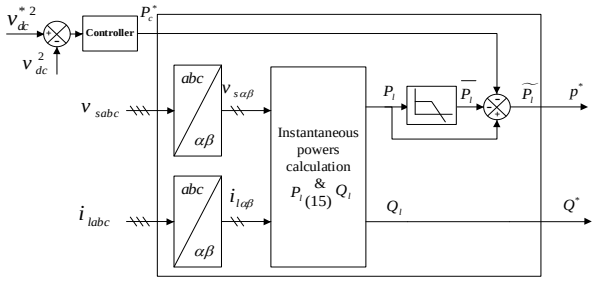

Fig. 4. Diagram of PQ technique for extracting of harmonic currents

B. Extraction of Harmonic voltages using PQ-PLL theory

It is comparable to PQ theory for currents and it has two parts, the first part is to extract voltage harmonics (17).

$$\begin{bmatrix} P_l \\ Q_l \end{bmatrix} = \begin{bmatrix} v_{l\alpha} & v_{l\beta} \\ v_{l\beta} & -v_{l\alpha} \end{bmatrix} \begin{bmatrix} i_{l\alpha} \\ i_{l\beta} \end{bmatrix} \tag{17}$$

The following equation is a possible way to express the powers:

$$\begin{cases} P_{fs}^* = \tilde{P}_l = P_l - \bar{P}_l \\ Q_{fs}^* = \tilde{Q}_l = Q_l - \bar{Q}_l \end{cases} \tag{18}$$

In the next second step, the voltage fall crossways the load must be determined.

$$\begin{bmatrix} \Delta v_{l\alpha} \\ \Delta v_{l\beta} \end{bmatrix} = \begin{bmatrix} v_{des\alpha} \\ v_{des\beta} \end{bmatrix} - \begin{bmatrix} v_{s\alpha} \\ v_{s\beta} \end{bmatrix} \tag{19}$$

The PQ-PLL theory's schematic diagram is shown in Figure (5).

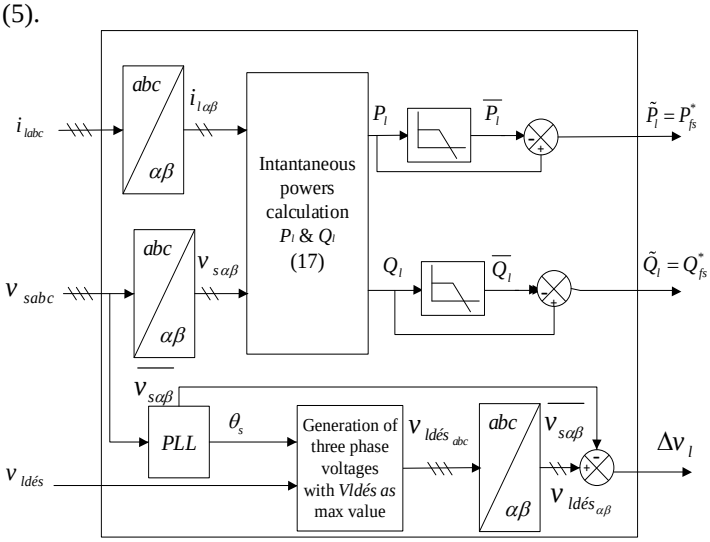

Fig. 5 Extracting of harmonic voltages with PQ-PLL technique

2.4 Synthesis of the backstepping controller (BC)

The idea behind the backtracking strategy is that some variables can be used as virtual controls to simplify the original high order system. Thus, using appropriate Lyapunov functions that provide global stability, the final control outputs can be established gradually [25].All control objectives are achieved using Lyapunov stability tools, unlike other approaches, which place limitations on the types of nonlinearities that can be utilized [26].

A. Synthesis of Boost BC

To get the most power out of the PV array, the backstepping control approach for the DC-DC boost converter is suggested. According to Fig. 3, two backstepping regulators are needed to regulate the PV generator's output voltage and current. By adjusting the voltage v_{pv} of the PV generator to a reference v_{pv}^* provided by the Perturb and Observe (P&O) MPPT

Algorithm, the boost converter's voltage is controlled. The inner loop current regulator's current reference i^*_{Lpv} is provided by the output of the voltage loop regulator and the PV current compensation. Therefore, the PV voltage v_{pv} , v_{dc} compensations, and the current control loop contribute to the converter's duty cycle.

The decomposition of the generic model provided by (13) into two subsystems yields the backstepping regulators required for the DC-DC boost converter as follows:

Subsystem 1:

$$\frac{dv_{pv}}{dt} = \frac{1}{C_{pv}} i_{pv} - \frac{1}{C_{pv}} i_{Lpv} \tag{20}$$

The PV output voltage v_{pv} is regarded as an output variable and the current i_{Lpv} as a variable control in the first subsystem.

Subsystem 2:

The PV current i_{Lpv} is regarded as an output variable and the duty cycle D is regarded as a variable control in the second subsystem covered by equation (21).

$$\frac{di_{Lpv}}{dt} = \frac{1}{L_{pv}} v_{pv} - \frac{1}{L_{pv}} (1-D) v_{dc} \tag{21}$$

Based on the first subsystem, which is identified by equation (20), the desired backstepping regulator of the voltage v_{pv} synthesis is examined as follows:

The formula for the variable error z_{vpv} is:

$$z_{vpv} = v^*_{pv} - v_{pv} \tag{22}$$

The dynamics of error z_{vpv} is:

$$\dot{z}_{vpv} = \dot{v}^*_{pv} - \left(\frac{1}{C_{pv}} i_{pv} - \frac{1}{C_{pv}} i^*_{Lpv} \right) \tag{23}$$

The potential Lyapunov function is :

$$V_{vpv} = \frac{1}{2} z^2_{vpv} \tag{24}$$

The derivative of (24) is:

$$\dot{V}_{vpv} = z_{vpv} \left(\dot{v}^*_{pv} - \left(\frac{1}{C_{pv}} i_{pv} - \frac{1}{C_{pv}} i^*_{Lpv} \right) \right) \tag{25}$$

The stability of the system is ensured when the derivative of the Lyapunov function is negative; this can be done by selecting the derivative of z_{vpv} as:

$$\dot{z}_{vpv} = -k_{vpv} z_{vpv} \tag{26}$$

Where, k_{vpv} is a positive constant.

Consequently, the equation for calculating the reference current i^*_{Lpv} is used (27).

$$i^*_{Lpv} = C_{pv} \dot{v}^*_{pv} - i_{pv} - k_{vpv} C_{pv} \left(v^*_{pv} - v_{pv} \right) \tag{27}$$

The second subsystem, described by equation (21), provides the foundation for the required backstepping regulator of the current i_{Lpv} synthesis and is examined as follows:

The expression "variable error z_{iLpv} " is defined by:

$$z_{iLpv} = i^*_{Lpv} - i_{Lpv} \tag{28}$$

Error dynamics z_{iLpv} is provided by:

$$\dot{z}_{iLpv} = \dot{i}^*_{pv} - \left(\frac{1}{L_{pv}} v_{pv} - \frac{1}{L_{pv}} \left(1 - D^* \right) v_{dc} \right) \tag{29}$$

The potential Lyapunov function is:

$$V_{iLpv} = \frac{1}{2} z^2_{iLpv} \tag{30}$$

The derivative of (30) is:

$$\dot{V}_{iLpv} = z_{iLpv} \left(\dot{i}^*_{pv} - \left(\frac{1}{L_{pv}} v_{pv} - \frac{1}{L_{pv}} \left(1 - D^* \right) v_{dc} \right) \right) \tag{31}$$

Selecting the derivative of z_{iLpv} as follows will assure the stability of the system:

$$\dot{z}_{iLpv} = -k_{iLpv} z_{iLpv} \tag{32}$$

Where, k_{iLpv} is a positive constant.

As a result, the equation's reference for duty cycle is determined (33).

$$D^* = \frac{1}{V_{dc}} \left(L_{PV} \dot{I}^*_{LPV} - V_{PV} + V_{dc} + L_{PV} k_{ILpv} \left(I^*_{LPV} - I_{LPV} \right) \right) \tag{33}$$

B. Synthesis of DC voltage BC

In the system represented by equation (34), the instantaneous active power P_c^* is regarded as a control variable, while the voltage v_{dc} is an output variable

$$\frac{dv_{dc}}{dt} = \frac{P_c}{v_{dc}C_{dc}} \tag{34}$$

A backstepping regulator is used to keep the DC-link voltage across the capacitor at a consistent, desired reference value. The tracking variable error z_{dc} is defined as follows in order to get the DC-link voltage follow its reference:

$$z_{dc} = v_{dc}^* - v_{dc} \tag{35}$$

Error dynamics z_{dv} is provided by:

$$\dot{z}_{dc} = \dot{v}_{dc}^* - \dot{v}_{dc} = \dot{v}_{dc}^* - \frac{P_c^*}{v_{dc}C_{dc}} \tag{36}$$

The following is the candidate Lyapunov function:

$$V_{vdc} = \frac{1}{2}z_{dc}^2 \tag{37}$$

The derivative of the function at (37) is denoted by:

$$\dot{V}_{vdc} = z_{dc}\left(\dot{v}_{dc}^* - \frac{P_c^*}{v_{dc}C_{dc}}\right) \tag{38}$$

Given that the Lyapunov function's derivative should be negative $\dot{V}_{vdc} < 0$, the stability of the system is ensured .

This may be done by using the derivative of z_{dc} as follows:

$$\dot{z}_{dc} = -k_{dc}z_{dc} \tag{39}$$

k_{dc} is a positive constant where.
The control law is then attained by:

$$P_c^* = v_{dc}C_{dc}\left(\dot{v}_{dc}^* + k_{dc}z_{dc}\right) \tag{40}$$

2.5 Predictive Direct Power Control (PDPC)

A. Synthesis of Parallel Powers PDPC

Using a predictive control technique, the PVG-UPQC average voltage vector is calculated, with instantaneous active and reactive powers being identical to their reference values at each sampling interval. This is the foundation of the proposed predictive DPC scheme. Instantaneous active and reactive power measurements and orders are therefore used as given input parameters in the block of predictive control technique.

as seen in figure (1). The PVG-UPQC average voltage vector $V_{fp\alpha\beta}$ is computed at the start of each sampling period T_e in order to allow cancellation of the instantaneous active and reactive power tracking errors at the end of the sampling period.

The control aim is then achieved with a constant switching frequency by creating a series of switching states using a space vector modulation approach.

The steps that must be taken to develop the predictive model that is needed for PDPC are illustrated below.

If the fundamental period is indefinitely short relative to the sample period T_e . The result of discretizing equations (3 and 9) is:

$$\begin{aligned} P_{fp}(k+1) - P_{fp}(k) &= \frac{T_e}{L_{fp}}(-R_{fp}P_{fp}(k) + V_{fp\alpha}(k)) \\ Q_{fp}(k+1) - Q_{fp}(k) &= \frac{T_e}{L_{fp}}(-R_{fp}Q_{fp}(k) + V_{fp\beta}(k)) \end{aligned} \tag{41}$$

Equation (41) may be rewritten as follows as the control goal is to make the values of references equal to real powers during the following sampling period:

$$\begin{aligned} P_{fp}^*(k+1) = P_{fp}(k+1) &= \frac{T_e}{L_{fp}}(-R_{fp}P_{fp}(k) + V_{fp\alpha}(k)) + P_{fp}(k) \\ Q_{fp}^*(k+1) = Q_{fp}(k+1) &= \frac{T_e}{L_{fp}}(-R_{fp}Q_{fp}(k) + V_{fp\beta}(k)) + Q_{fp}(k) \end{aligned} \tag{42}$$

The necessary PVG-UPQC average voltage vector is expressed using (42), as follows:

$$\begin{aligned} V_{fp\alpha}(k) &= R_{fp}P_{fp}(k) + \frac{L_{fp}}{T_e}(P_{fp}^*(k+1) - P_{fp}(k)) \\ V_{fp\beta}(k) &= R_{fp}Q_{fp}(k) + \frac{L_{fp}}{T_e}(Q_{fp}^*(k+1) - Q_{fp}(k)) \end{aligned} \tag{43}$$

From figure (6), a linear extrapolation may be employed to approximate the references of power at the next sampling time (k+1).

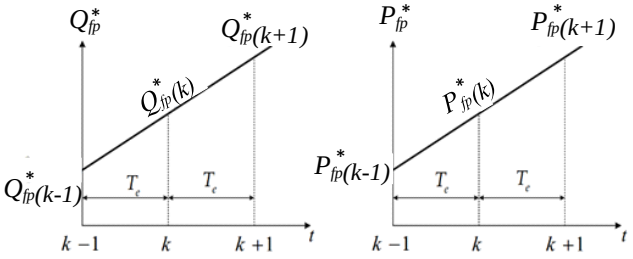

Fig. 6.Predictive reference powers evaluation

The references of the expected power:

$$\begin{aligned} P_{fp}^*(k+1) &= 2P_{fp}^*(k) - P_{fp}^*(k-1) \\ Q_{fp}^*(k+1) &= 2Q_{fp}^*(k) - Q_{fp}^*(k-1) \end{aligned} \tag{44}$$

For the duration of the period of each sampling, equation (45) gives the digital PDPC control rule that produces the necessary SAPF average voltage vector:

$$\begin{aligned} V_{fp\alpha}^*(k) &= R_{fp}P_{fp}(k) + \frac{L_{fp}}{T_e}(\Delta P_{fp}^*(k) + e_{P_{fp}}(k)) \\ V_{fp\beta}^*(k) &= R_{fp}Q_{fp}(k) + \frac{L_{fp}}{T_e}(\Delta Q_{fp}^*(k) + e_{Q_{fp}}(k)) \end{aligned} \tag{45}$$

The tracking errors of power are $e_{P_{fp}}(k)$ and $e_{Q_{fp}}(k)$:

$$\begin{aligned} e_{P_{fp}}(k) &= P^*_{fp}(k) - P_{fp}(k) \\ e_{Q_{fp}}(k) &= Q^*_{fp}(k) - Q_{fp}(k) \end{aligned} \tag{46}$$

The real change in both powers is represented by the references $\Delta P^*_{fp}(k)$ and $\Delta Q^*_{fp}(k)$:

$$\begin{aligned} \Delta P^*_{fp}(k) &= P^*_{fp}(k) - P^*_{fp}(k-1) \\ \Delta Q^*_{fp}(k) &= Q^*_{fp}(k) - Q^*_{fp}(k-1) \end{aligned} \tag{47}$$

The reference voltages $v^*_{fp\alpha}$ and $v^*_{fp\beta}$ may be computed using formula (4) as shown below previously the voltages $V^*_{fp\alpha}$ and $V^*_{fp\beta}$ have been acquired.

$$v^*_{fp\alpha} = \frac{v_{s\alpha}}{v^2_{s\alpha} + v^2_{s\beta}} V^*_{fp\alpha} - \frac{v_{s\beta}}{v^2_{s\alpha} + v^2_{s\beta}} V^*_{fp\beta} + v_{s\alpha} \tag{48}$$

$$v^*_{fp\beta} = \frac{v_{s\beta}}{v^2_{s\alpha} + v^2_{s\beta}} V^*_{fp\alpha} + \frac{v_{s\alpha}}{v^2_{s\alpha} + v^2_{s\beta}} V^*_{fp\beta} + v_{s\beta} \tag{49}$$

B. Synthesis of Series powers PDPC

For tracking, the control law is:

$$\begin{aligned} V^*_{fs\alpha}(k) &= R_{fs} P_{fs}(k) + \frac{L_{fs}}{T_e}(\Delta P^*_{fs}(k) + e_{P_{fs}}(k)) \\ V^*_{fs\beta}(k) &= R_{fs} Q_{fs}(k) + \frac{L_{fs}}{T_e}(\Delta Q^*_{fs}(k) + e_{Q_{fs}}(k)) \end{aligned} \tag{50}$$

$$v^*_{fs\alpha} = \frac{v_{inj\alpha}}{v^2_{inj\alpha} + v^2_{inj\beta}} V^*_{fs\alpha} - \frac{v_{inj\beta}}{v^2_{inj\alpha} + v^2_{inj\beta}} V^*_{fs\beta} + v_{inj\alpha} \tag{51}$$

$$v^*_{fs\beta} = \frac{v_{inj\beta}}{v^2_{inj\alpha} + v^2_{inj\beta}} V^*_{fs\alpha} + \frac{v_{inj\alpha}}{v^2_{inj\alpha} + v^2_{inj\beta}} V^*_{fs\beta} + v_{inj\beta} \tag{52}$$

2.6 Modulation of Three-level Space Vector

The three-level SVM technique used to generate the switch PWM control signals is described in this section (sa, sb and sc). Figure (7) depicts the space vector for a three-level inverter in α-β frame. There are three zero states in the centre, twelve inside hexagons and twelve outer hexagons , for a total of 27 states. The output voltage for these states can take one of three values: ' $v_{dc}/2$', '0' and '- $v_{dc}/2$' accordingly.

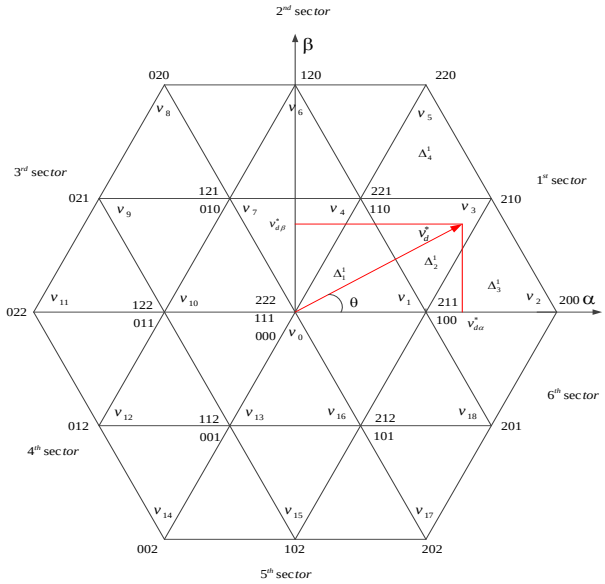

Fig. 7.design of three-level Space-vector

As seen in Figure (8), there are four triangular zones in each section. The space vector modulation is used in order to rebuild the reference voltage vector from its three neighboring vectors, where this vector is equivalent to the total of these different vectors. Finding the reference voltage vector must thus be the first step. It is possible to divide this process into two parts, the first of which determines the sector number and the second of which determines the triangle where the vector is inserted [20][24].

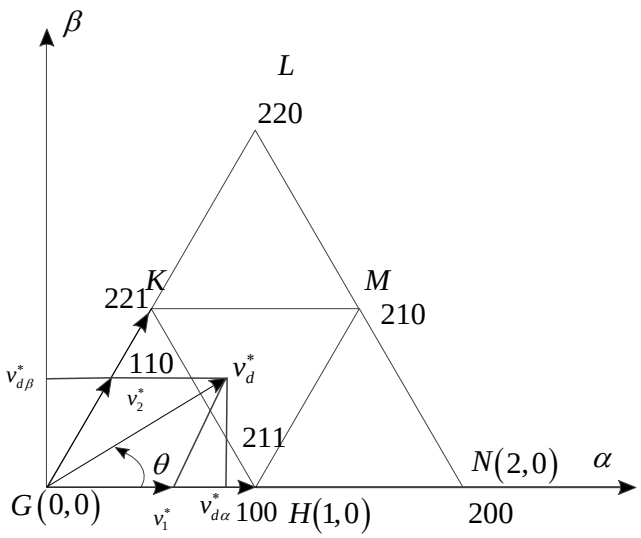

Fig. 8.Configuration of Vector in initial sector

The reference voltage vector's magnitude and angle are calculated as shown in Figure (8) as follows:

$$v^*_d = \sqrt{v^{*2}_{d\alpha} + v^{*2}_{d\beta}} \tag{53}$$

$$\theta = \tan 2^{-1}\left(\frac{v^*_{d\beta}}{v^*_{d\alpha}}\right) \tag{54}$$

a) First Step: Sector Determination

The following equation contains the sector numbers:

$$S = ceil(\frac{\theta}{\pi/3}) \in \{1,2,3,4,5,6\} \quad (55)$$

Where *ceil* is a function that increases an integer by one when it rounds a number

b) Second Step: Triangle Identification

On the two axes doing $\pi/3$ rad between them, the reference vector is projected. Equations (56) and (57) standardize the predicted components as follows:

$$v_1^{*S} = 2\frac{v_d^*}{\sqrt{2/3}v_{dc}}\left(\cos(\theta-(S-1)\frac{\pi}{3})-\frac{1}{\sqrt{3}}\sin(\theta-(S-1)\frac{\pi}{3})\right) \quad (56)$$

$$v_2^{*S} = 2\frac{v_d^*}{\sqrt{2/3}v_{dc}}\left(\frac{2}{\sqrt{3}}\sin(\theta-(S-1)\frac{\pi}{3})\right) \quad (57)$$

For finding the triangles number in a sector S, it is necessary to define the two integers:

$$\begin{aligned} l_1^S &= \text{int}\left(v_1^{*S}\right) \\ l_2^S &= \text{int}\left(v_2^{*S}\right) \end{aligned} \quad (58)$$

int is a function in which a number is rounding to the nearest integer near zero.

As exposed in figure (9), If the vector of reference is located in the parallelogram composed by the vertices G, K, H and M, the two integers l_1^S and l_2^S should validated the condition: $l_1^S = 1$ and $l_2^S = 2$

To verify the reference vector situated in the triangle shaped by the vertices H, K, G or in that shaped by the vertices M, K, H, one of the situations should be confirmed:

v_d^{*S} is positioned in GHK triangle if:

$$v_1^{*S} + v_2^{*S} < l_1^S + l_2^S + 1 \quad (59)$$

v_d^{*S} is positioned in HKM triangle if:

$$v_1^{*S} + v_2^{*S} \geq l_1^S + l_2^S + 1 \quad (60)$$

With the similar process, the numbers of other triangles in every sector can be determined.

c) computation of Duration Times

If the reference vector is positioned in HKM triangle, it is restructured from the three neighboring vectors $v_x^{\Delta_i^S}$, $v_y^{\Delta_i^S}$ and $v_z^{\Delta_i^S}$ using the following relation:

$$\begin{aligned} v_x^{\Delta_i^S} t_x^{\Delta_i^S} + v_y^{\Delta_i^S} t_y^{\Delta_i^S} + v_z^{\Delta_i^S} t_z^{\Delta_i^S} &= v_d^* T_s \\ t_x^{\Delta_i^S} + t_y^{\Delta_i^S} + t_z^{\Delta_i^S} &= T_s \end{aligned} \quad (61)$$

Where $t_x^{\Delta_i^S}$, $t_y^{\Delta_i^S}$ and $t_z^{\Delta_i^S}$ are the duration times of vectors and x, y and z are the vertices of G, H and K .

In the frame constituted of two axes in which the angle between them is 60^o the projection of (56) gives the following:

$$\begin{aligned} v_{x1}^{\Delta_i^S} t_x^{\Delta_i^S} + v_{y1}^{\Delta_i^S} t_y^{\Delta_i^S} + v_{z1}^{\Delta_i^S} t_z^{\Delta_i^S} &= v_1^{*S} T_s \\ v_{x2}^{\Delta_i^S} t_x^{\Delta_i^S} + v_{y2}^{\Delta_i^S} t_y^{\Delta_i^S} + v_{z2}^{\Delta_i^S} t_z^{\Delta_i^S} &= v_2^{*S} T_s \\ t_x^{\Delta_i^S} + t_y^{\Delta_i^S} + t_z^{\Delta_i^S} &= T_s \end{aligned} \quad (62)$$

The vertices coordinates M, N , G, K, H and L are expressed by the equation:

$$\begin{aligned} \left(v_{G1}^{\Delta_i^S}, v_{G2}^{\Delta_i^S}\right) &= (0,0), & \left(v_{H1}^{\Delta_i^S}, v_{H2}^{\Delta_i^S}\right) &= (1,0) \\ \left(v_{N1}^{\Delta_i^S}, v_{N2}^{\Delta_i^S}\right) &= (2,0), & \left(v_{K1}^{\Delta_i^S}, v_{K2}^{\Delta_i^S}\right) &= (0,1) \\ \left(v_{M1}^{\Delta_i^S}, v_{M2}^{\Delta_i^S}\right) &= (1,1), & \left(v_{L1}^{\Delta_i^S}, v_{L2}^{\Delta_i^S}\right) &= (0,2) \end{aligned} \quad (63)$$

By replacement the coordinates of v_x, v_y, v_z demonstrated in (63) in (62), in each triangle, the time period in sector s for each triangle are cited in Table (I).

Table 1. Time period in sector s for each triangle

Number of Triangle	Period of time		
	$t_x^{\Delta_i^S}$	$t_y^{\Delta_i^S}$	$t_z^{\Delta_i^S}$
$\Delta_1^S(G,H,K)$	$T_s - t_y^{\Delta_i^S} - t_z^{\Delta_i^S}$	$v_1^{*S} T_s$	$v_2^{*S} T_s$
$\Delta_2^S(M,K,H)$	$T_s - t_y^{\Delta_i^S} - t_z^{\Delta_i^S}$	$\left(1-v_1^{*S}\right)T_s$	$\left(1-v_2^{*S}\right)T_s$
$\Delta_3^S(H,N,M)$	$T_s - t_y^{\Delta_i^S} - t_z^{\Delta_i^S}$	$\left(v_1^{*S}-1\right)T_s$	$v_2^{*S} T_s$
$\Delta_4^S(K,M,L)$	$T_s - t_y^{\Delta_i^S} - t_z^{\Delta_i^S}$	$v_1^{*S} T_s$	$\left(v_2^{*S}-1\right)T_s$

In the second triangle, the vectors appliance times are givenin equation (64) when the vector coordinates $v_x^{\Delta_i^s} = v_G^{\Delta_i^s}$, $v_x^{\Delta_i^s} = v_H^{\Delta_i^s}$ and $v_x^{\Delta_i^s} = v_K^{\Delta_i^s}$ are substituted in equation (62).

$$\begin{aligned} t_y^{\Delta_i^s} &= (v_1^{*s}-1)T_s \\ t_z^{\Delta_2^s} &= (v_2^{*s}-1)T_s \\ t_x^{\Delta_i^s} &= T_s - (t_y^{\Delta_i^s} - t_z^{\Delta_i^s}) \end{aligned} \quad (64)$$

d) Energy Minimization Based Balancing DC Capacitor Voltages

The combined energy of the two capacitors in a three-level diode-clamped converter is provided in [9]:

$$E = \frac{1}{2}\sum_{i=1}^{2} C_i v_{ci}^2 \quad (65)$$

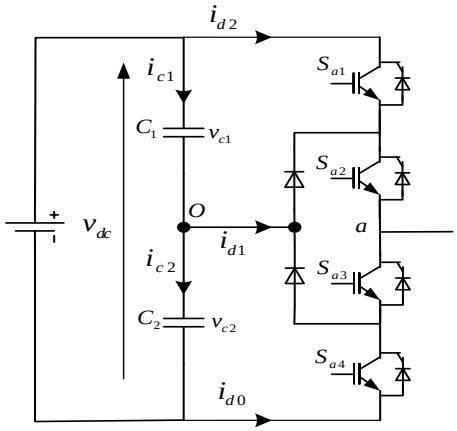

Fig. 9.Three-level diode-clamped inverter cell.

The total energy E decreases to its lowest value ($E_{\min}$) when the voltages of the two capacitors are balanced, providing that the two capacitors have equal capacitances, *C1 = C2 = C*. Following is the minimal total energy:

$$E_{\min} = \frac{C}{2}\frac{v_{dc}^2}{2} \tag{66}$$

The ability to minimize energy can be utilized to balance capacitor voltages. Due to this, the following cost function J is established using the quadratic sum of the voltages v_{ci} and reference value differences:

$$J = \frac{1}{2}C\sum_{i=2}^{n-1}\left(v_{ci} - \frac{v_{dc}}{2}\right)^2 \tag{67}$$

The function J may be decreased to zero based on an appropriate selection of redundant vectors, maintaining the capacitor voltages at their reference levels. The formula that guarantees that the cost function J will converge to its smallest value is as follows:

$$\frac{dJ}{dt} = \sum_{i=1}^{2}\Delta v_{ci} i_{ci} \le 0 \tag{68}$$

where i_{ci} represents the capacitor's current C_i, $i = 1,2$

The currents of DC-side intermediary section i_{d0} and i_{d1} have an impact on these DC-capacitor currents. Equation (68) can be expressed by i_{d0} . i_{d1} . i_{ci} and it can be written as follows:

$$\begin{aligned} i_{c1} &= -i_{d1} \\ i_{c2} &= -i_{d1} - i_{d0} \end{aligned} \tag{69}$$

The requirement to attain the balancing of voltage is determined in (70) by substituting the values of i_{c1} and i_{c2} from equation (68) in (69):

$$-\Delta v_{c1} i_{d1} - \Delta v_{c2}\left(i_{d0} + i_{d1}\right) \le 0 \tag{70}$$

The following condition is confirmed when the continuous connection voltages v_{c1}, v_{c2} are near to v_{dc}^*:

$$\Delta v_{c1} + \Delta v_{c2} = 0 \tag{71}$$

Equation (70) may be used to represent equation (69) as follows:

$$\Delta v_{c2} i_{d0} \ge 0 \tag{72}$$

Equation (72) gives the following results when the averaging operator is applied over a single sampling period:

$$\frac{1}{T}\int_{kT}^{(k+1)T}\left(\Delta v_{c2} i_{d0}\right)dt \ge 0 \tag{73}$$

Assuming the sampling period T, as contrasted to the time interval associated with the dynamics of capacitor voltages, is appropriately small, the capacitor voltages may be considered to remain constant across one sample period; accordingly, the equation (73) is reduced to:

$$\Delta v_{c2}(k)\overline{i_{d0}} \ge 0 \tag{74}$$

Where $\overline{i_{d0}}$ is the averaged value of the i_{d0}, and $\Delta v_{c2}(k)$ is the drift voltage at the sampling period. Therefore, just one DC capacitor voltage has to be detected in order to manage DC-capacitor voltages. Control is made incredibly easy and dependable by this function. The optimal combination that optimizes equation (74) should be chosen after computing the current $\overline{i_{d0}}$ for various combinations of nearby redundant switching states throughout a sampling interval.

2.7 Configuration of Comparative PI controller

To demonstrate the effectiveness of the proposed BC-PDPC, its performance is compared to that of the PI regulator.

By regulating the active power flow between the PCC and the DC bus, the DCPI regulator's function is to enable tracking the reference.

The following transfer function is calculated from equation (8):

$$\frac{v_{dc}^2(s)}{P_c(s)} = \frac{2}{C_{dc}s} \tag{75}$$

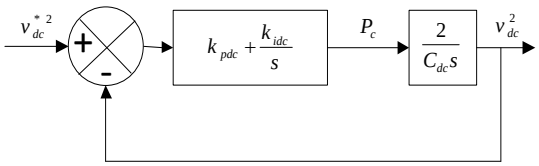

Fig. 10.Regulation of continuous voltage.

The closed loop transfer function is illustrated in:

$$G(s) = \frac{v_{dc}^2(s)}{v_{dc}^{*2}(s)} = \frac{\frac{2k_{pdc}}{C_{dc}}s + \frac{2k_{idc}}{C_{dc}}}{s^2 + \frac{2k_{pdc}}{C_{dc}}s + \frac{2k_{idc}}{C_{dc}}} \tag{76}$$

From (76), at ransfer function (77) can be obtained:

$$H(s) = \frac{2\zeta\omega_n s + \omega_n^2}{s^2 + 2\zeta\omega_n s + \omega_n^2} \tag{77}$$

It can be found:

$$\begin{aligned} k_{idc} &= C_{dc}\omega_n^2 / 2 \\ k_{pdc} &= \xi\omega_n C_{dc} \end{aligned} \tag{78}$$

$\omega_n = 2\pi f_n$ is the Natural pulsatance of the regulator and $0 < \xi < 1$ is the damping factor for a good dynamic and acceptable oscillations, $f_n = 25Hz$ $\xi = 0.7$ are choosen.

The PI coefficients of currents, voltages, and Boost controllers may also be obtained using the same procedure and are listed below.

TABLEII
PI PARAMETERS

Coefficients	Value
K_{ipv}	4.60
K_{idc}	0.1
K_{ppv}	0,45 10^2
k_{pfs}	0.30
K_{ifs}	10.0
k_{pfp}	3.50
K_{ifp}	3,55 10^2
k_{pdc}	0,088 10^{-2}

III. DISCUSSION OF RESULTS

In order to improve the efficacy of the proposed control for ThePVG-UPQC performance assessment, the voltage filtering and harmonic current and finally the compensation of reactive power, MATLAB/Simulink is used to install a model includes all parameters cited in the following table.

TABLEIII
SYSTEM PARAMETERS

Parameter	value
R_d , L_d	15.0 Ω, 2 mH
R_{fp}, L_{fp}	20.0 mΩ, 2.50 mH
k_{dc}	250.0
R_{fs}, L_{fs},C_{fs}	1.50 Ω, 3 mH, 0.10 mF
L_{pv},C_{pv}	5.0 mH, 55.0 mF
the source voltage RMS value	220.0 V
f_s	12.0 kHz
R_l, L_l	10.0 mΩ, 0.30 µH
k_{p1}= k_{p2}	1120.0
V_{dc}^*	900.0 V
Rs, Ls	3.0mΩ, 2.60 µH
PV array P_{pv}, V_{mp},I_{mp}, I_{sc},V_{oc}	150W,34.50V,4.35A. 4.75A, 43.50V
k_{s1}= k_{s2}	1150.0
K_{b1}= k_{b2}	1450.0
C_{dc}	8.0 mF

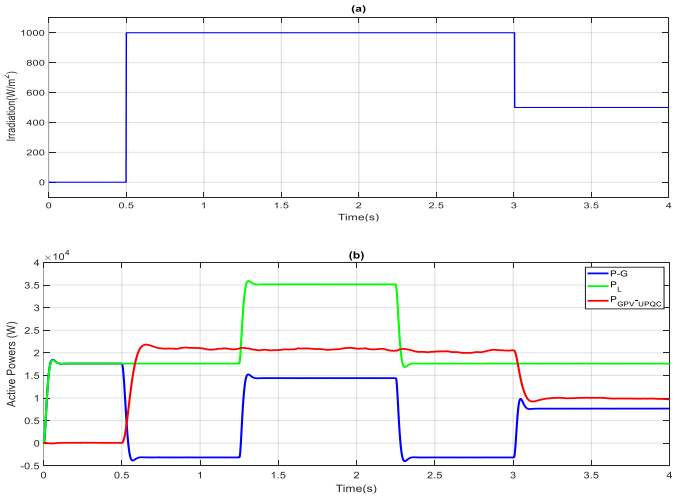

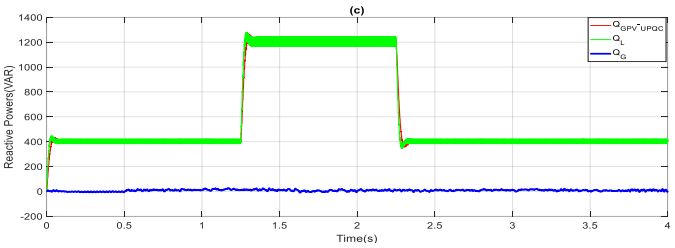

Fig. 11. Different results during conditions variation of the proposed regulator

The profile of the irradiation chosen is shown in Fig. 11.a at 25 °C. Initial irradiation is absent (t<0.5s), and the PVG-UPQC is only regulated to filter harmonics and make up for reactive power, whereas the load is supplied by the network (17.5 kW). When the irradiation is attuned to 1000 W/m2, the maximum power that can be injected is around 21 kW. the generated power is greater corresponding to that needed by the load,so in this situation, the GPV-UPQC control is injecting power to the network from the moment 0.50s to 1.250s for first compensating reactive power, second for filtering harmonics, and finally is to supply the load as illustrated in Fig. 11(b) and (c). It is noticed that from these results, the consumption of active power is about 17.5 kW and reactive one is around 400 VAR is equivalent to the total of the GPV-UPQC and grid power supplies.

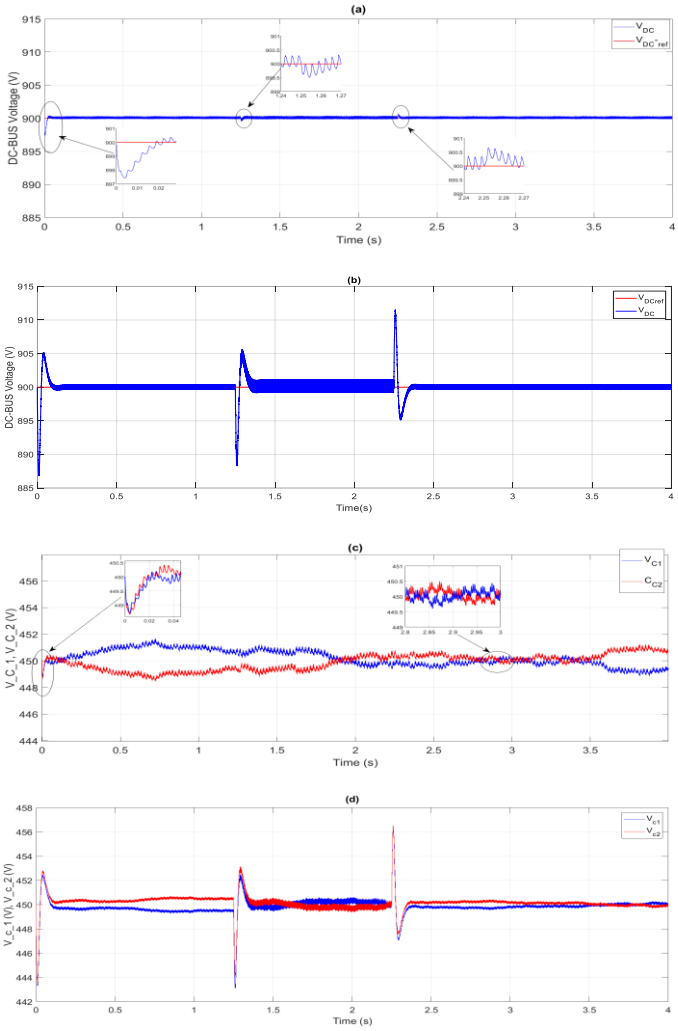

Fig. 12. Simulation results under conditions and load variation a):DC-link voltage v_{dc} with B-PDPC, b):DC-link voltage $v_{dc}$with PI regulator, c):DC capacitors voltages with B-PDPC, d):DC capacitors voltages with PI regulator.

Figs. 12 show DC-link voltage vdc, and DC capacitors voltages respectively. The DC-link voltage is little impacted by load change (approximately 2V), and it recovers in about 0.08s (see Fig. 12(a) and (c)). As further evidence of the success of the three-level SVM based on a balancing method, it can also be seen that the DC capacitor voltages are balancing at their reference levels (450 V) with minimal ripple around the balance point.

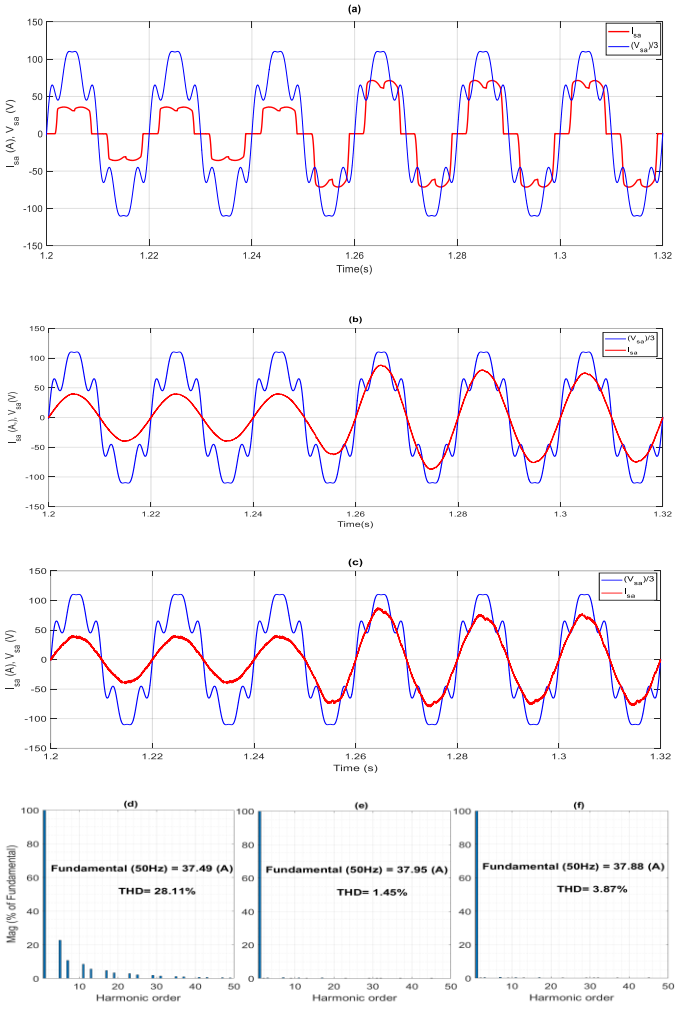

Fig. 13Simulation results under load variation.

Figs. 12 and 13 show the dynamic behavior under a sudden change in load caused by introducing a second load at the moment t =1.25s for 1 s. It is obvious that after introducing the control, the current of grid is very well sinusoidal, and even in this transient situation, the aim of unity power factor is effectively attained. Figs. 13(a) and (b) show the phase source voltage with source current with B-PDPC before and after compensation and Figs. 13(d) and (e) present source current harmonic spectrum before and after compensation with B-PDPC and finally Fig . 13(f) illustrate after compensation source current harmonic spectrum with PI regulator. Figs. 13 (d), (e), and (f) display the spectrum analysis of the voltage of the load and the AC grid current with and without compensation for the current. it is noticed that from these results, the proposed control present perfect effectiveness to obtain the wanted objectives.

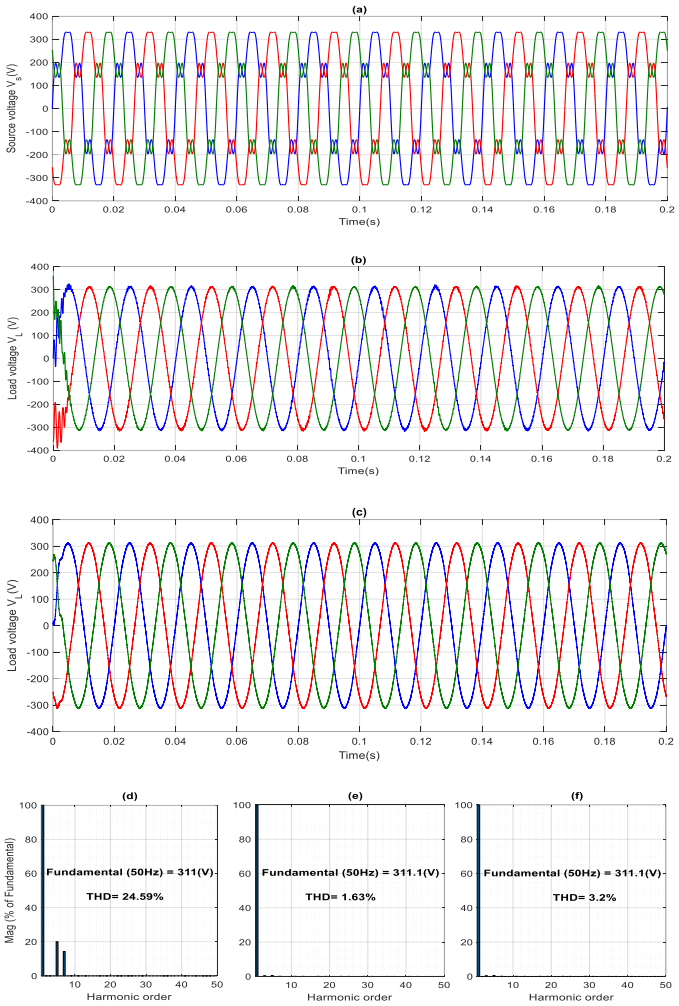

Fig. 14. Simulation results under source voltage perturbation.

Figs. 14. (a), (b), and (c) present Voltage of the load before compensation, after compensation with PI regulator and with B-PDPC respectively. Figs. 14. (d), (e), and (f) display the spectrum analysis of the voltage for both controllers. It demonstrates that the THD in the grid currents is reduced by the PVG-UPQC from 28.11% to 3.87% using the conventional PI regulator. A backstepping-based PDPC regulator, however, reduces the present THD to 1.45%. The THD of load voltage falls to 3.20% from 24.58% with PI, and further drops with B-PDPC to 1.63%, demonstrating the effectiveness of the created nonlinear regulator.

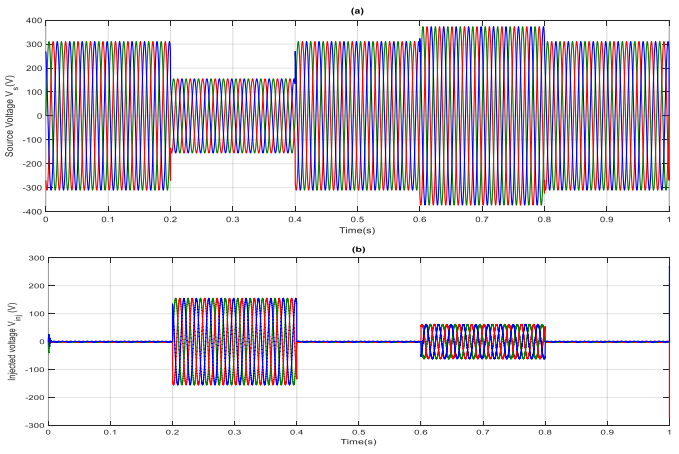

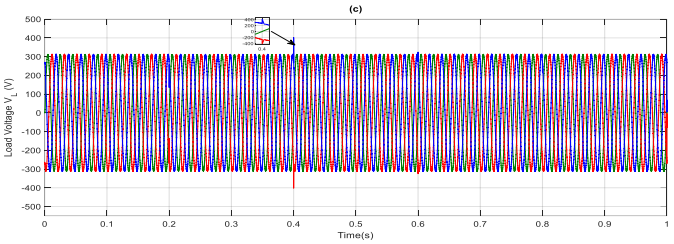

Fig. 15.Examination of voltage (sag and swell) with B-PDPC.

Figs. 15.a and 15.b present the profile of disturbed source voltage and the voltage of compensation during perturbation respectively. From these examinations, in sag voltage situation, the PVG-UPQC swiftly injects components of equal positive voltage that are phase-locked to the grid voltage, and in voltage swell situation, the PVG-UPQC injects negative voltage components in the opposite phase of the grid voltage to obtain the voltage of the load near to its regular value, as shown in Fig. 15.c.

The load voltage is once again rapidly determined to be extremely near to a sinusoidal voltage when the PVG-UPQC is experienced with sag and swell in the voltage of network. To maintain a constant load voltage, the PVG-UPQC can therefore give the necessary compensating voltage components.

Rapidity and minimal THD with the lack of an overshoot in the response of continuous bus voltage throughout fluctuation of load, demonstrate the superiority and efficacy of the backstepping-based PDPC regulator over the more conventional linear PI regulator shown in the following table:

TABLEIII
COMPARISONOF PI CONTROLLER WITH SLIDING MODE CONTROLLER

Factor	PI controller	BC-PDPC controller
THDv (%)	3.2	1.63
Overshoot	+	-
THDi (%)	3.87	1.45
DC link charging (s)	0.110	0.08

IV. CONCLUSION

In this present study, a PVG-UPQC control plan is implemented, which includes techniques for harmonic extraction for both currents and voltages and also its mathematical model. To reduce current and voltage harmonics, a backstepping-PDPC regulator is developed. Because of its advantages in terms of implementation at a fixed frequency, a three-level SVM with energy minimization based balancing DC capacitor voltages is utilized for the closing power switches management. The simulation's findings show that the source side currents and load side voltages exhibit a sinusoidal form throughout the whole system's operation. These findings unequivocally demonstrate that PVG-UPQC controlled by backstepping-PDPC performs far better than traditional regulators.

REFERENCES

[1] M. Hari Prabhu, K. Sundararaju,"Power quality improvement of solar power plants in grid connected system using novel Resilient Direct Unbalanced Control (RDUC) technique", Microprocessors and Microsystems, Volume 75, 2020, 103016, ISSN 0141-9331.

[2] J.C. Hernandez, F.J. Ruiz-Rodriguez, F. Jurado, F. Sanchez-Sutil,"Tracing harmonic distortion and voltage unbalance in secondary radial distribution networks with photovoltaic uncertainties by an iterative multiphase harmonic load flow", Electric Power Systems Research,Volume 185, 2020, 106342, ISSN 0378-7796.

[3] Buddhadeva Sahoo, Mohammed M. Alhaider, Pravat Kumar Rout, "Power quality and stability improvement of microgrid through shunt active filter control application: An overview",Renewable Energy Focus,Volume 44,2023,Pages 139-173,ISSN 1755-0084,https://doi.org/10.1016/j.ref.2022.12.006.

[4] N. Patnaik, A. K. Panda, "Performance analysis of a 3 phase 4 wire UPQC system based on PAC based SRF controller with real time digital simulation", International Journal of Electrical Power & Energy Systems, Volume 74. January 2016, pp. 212-221.

[5] Carlos Gurrola-Corral, Juan Segundo, Miguel Esparza, Roel Cruz,"Optimal LCL-filter design method for grid-connected renewable energy sources", International Journal of Electrical Power & Energy Systems, Volume 120, 2020, 105998, ISSN 0142-0615.

[6] R. Hemalatha, M Ramasamy, "Microprocessor and PI controller based three phase CHBMLI based DSTATCOM for THD mitigation using hybrid control techniques", Microprocessors and Microsystems, Volume 76, 2020, 103093,ISSN 0141-9331.

[7] Vinícius Dário Bacon, Sérgio Augusto Oliveira da Silva, Josep M. Guerrero, "Multifunctional UPQC operating as an interface converter between hybrid AC-DC microgrids and utility grids", International Journal of Electrical Power & Energy Systems, Volume 136, 2022,107638, ISSN 0142-0615.

[8] DAHDOUH, ADEL, Barkat, Said, Aissa, Chouder,"A Combined Sliding Mode Space vector Modulation Control of the Shunt Active Power Filter Using Robust Harmonic Extraction Method A Combined Sliding Mode Space vector Modulation Control of the Shunt Active Power Filter Using Robust Harmonic Extraction Method". Algerian Journal of Signals and Systems. Vol. 1, 2016, pp. 37-46. 10.51485/ajss.v1i1.17.

[9] M. Bouzidi, A. Benaissa, S. Barkat, "Application of feedback linearization to the virtual flux direct power control of three-level three-phase shunt active power filter", International review of electrical engineering, Vol. 5, No. 3, pp.1128-1140, 2012.

[10] T. Koroglu, A. Tan, M. M. Savrun, M. U. Cuma, K. C. Bayindir and M. Tumay, "Implementation of a Novel Hybrid UPQC Topology Endowed With an Isolated Bidirectional DC–DC Converter at DC link," in IEEE Journal of Emerging and Selected Topics in Power Electronics, vol. 8, no. 3, pp. 2733-2746, Sept. 2020, doi: 10.1109/JESTPE.2019.2898369.

[11] R. H. Yang and J. X. Jin, "Unified Power Quality Conditioner With Advanced Dual Control for Performance Improvement of DFIG-Based Wind Farm," in IEEE Transactions on Sustainable Energy, vol. 12, no. 1, pp. 116-126, Jan. 2021, doi: 10.1109/TSTE.2020.2985161.

[12] S. Devassy and B. Singh, "Performance Analysis of Solar PV Array and Battery Integrated Unified Power Quality Conditioner for Microgrid Systems," in IEEE Transactions on Industrial Electronics, vol. 68, no. 5, pp. 4027-4035, May 2021, doi: 10.1109/TIE.2020.2984439.

[13] M. A. Mansor, K. Hasan, M. M. Othman, S. Z. B. M. Noor and I. Musirin, "Construction and Performance Investigation of Three-Phase Solar PV and Battery Energy Storage System Integrated UPQC," in IEEE Access, vol. 8, pp. 103511-103538, 2020, doi: 10.1109/ACCESS.2020.2997056.

[14] J. Yu, Y. Xu, Y. Li and Q. Liu, "An Inductive Hybrid UPQC for Power Quality Management in Premium-Power-Supply-Required Applications," in IEEE Access, vol. 8, pp. 113342-113354, 2020, doi: 10.1109/ACCESS.2020.2999355.

[15] Nishant Patnaik, Anup Kumar Panda,"Performance analysis of a 3 phase 4 wire UPQC system based on PAC based SRF controller with real time digital simulation", International Journal of Electrical Power & Energy Systems, Volume 74, 2016, Pages 212-221, ISSN 0142-0615.

[16] S. A. O. da Silva, L. B. G. Campanhol, G. M. Pelz and V. de Souza, "Comparative Performance Analysis Involving a Three-Phase UPQC Operating With Conventional and Dual/Inverted Power-Line Conditioning Strategies," in IEEE Transactions on Power Electronics, vol. 35, no. 11, pp. 11652-11665, Nov. 2020, doi: 10.1109/TPEL.2020.2985322..

[17] S. Poongothai, S. Srinath, "Power quality enhancement in solar power with grid connected system using UPQC", Microprocessors and Microsystems, Volume 79, 2020, 103300, ISSN 0141-9331.

[18] S. J. Alam and S. R. Arya, "Control of UPQC based on steady state linear Kalman filter for compensation of power quality problems," in

Chinese Journal of Electrical Engineering, vol. 6, no. 2, pp. 52-65, June 2020, doi: 10.23919/CJEE.2020.000011.

[19] A. Ozdemir.and Z. Ozdemir., "Digital current control of a three-phase four-leg voltage source inverter by using p-q-r theory" Power Electronics, IET , Vol.7, No.3, March 2014, pp.527-539.

[20] Shivinder Mehta, Vinod Puri, "A review of different multi-level inverter topologies for grid integration of solar photovoltaic system",Renewable Energy Focus,Volume 43,2022,Pages 263-276,ISSN 1755-0084,https://doi.org/10.1016/j.ref.2022.10.002..

[21] S. Lakshmi Kanthan Bharathi, S. Selvaperumal, MGWO-PI controller for enhanced power flow compensation using unified power quality conditioner in wind turbine squirrel cage induction generator, Microprocessors and Microsystems, Volume 76, 2020, 103080, ISSN 0141-9331.

[22] S. K. Dash and P. K. Ray, "A New PV-Open-UPQC Configuration for Voltage Sensitive Loads Utilizing Novel Adaptive Controllers," in IEEE Transactions on Industrial Informatics, vol. 17, no. 1, pp. 421-429, Jan. 2021, doi: 10.1109/TII.2020.2986308.

[23] R. Guzman, L.G Vicuna,J. Morales, M. Castilla, J. Matas,. "Sliding-Mode Control for a Three-Phase Unity Power Factor Rectifier Operating at Fixed Switching Frequency" in Power Electronics, IEEE Transactions on , vol.31, no.1, Jan. 2016, pp.758-769.

[24] A. Chebabhi,M.K Fellah and M.F Benkhoris "Sliding Mode Controller for Four Leg ShuntActive Power Filter to Eliminating ZeroSequence Current, Compensating Harmonics and Reactive Power with Fixed Switching Frequency ", Serbian Journal Of Electrical Engineering, Vol. 12, No. 02, june 2015, pp. 205- 218.

[25] K.Ramya and R.Prakash "Comparative Analysis of PWM Techniques for Three Level Diode Clamped Voltage Source Inverter", International Journal of Power Electronics and Drive System, Vol. 5, No. 01, July-2014, pp. 15- 23.

[26] J. Han, X. Li, Y. Jiang and S. Gong, "Three-Phase UPQC Topology Based on Quadruple-Active-Bridge," in IEEE Access, vol. 9, pp. 4049-4058, 2021, doi: 10.1109/ACCESS.2020.3047961.

[27] Ali Reza Reisi, Mohammad H. Moradi, Hemen Showkati, Combined photovoltaic and unified power quality controller to improve power quality, Solar Energy, Volume 88, 2013, Pages 154-162, ISSN 0038-092X.

BIOGRAPHIES

Lakhdar MAZOUZ, is an assistant lecturer and researcher at the department of Electrical Engineering at university of Djelfain, Algeria. He received his Licence degree in electrical engineering from university of Laghouat in Algeria. Also, he received the Magister (in 2010) as well as PhD degree (in 2017) from the Djillali Liabes university of Sidi Bel-Abbes (Algeria). His main research interests are: the VSC-HVDC link, the FACTS and the Offshore Wind Farms.

Adel DAHDOUH received his License and Master degrees in Electrical Engineering from Mohamed Boudiaf University of M'sila, Algeria, in 2013 and 2015 respectively. Currently, he is a researcher in Applied Automation and Industrial Diagnosticsat university ofDjelfa (LAADI). His research interest includes control of power converters, power quality enhancement, micro-grids and energy management systems.

Brahim Elkhalil YOUCEFA received his License and Master degrees in Electrical Engineering at Mohamed Boudiaf university of M'sila inAlgeriain 2013 and 2015 respectively. He received the PhD degree in 2020 from the Djillali Liabes university of Sidi Bel-Abbes (Algeria). His research interest includes the control of power converters, power quality and modeling and control of renewable energy sources.